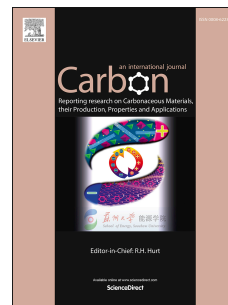


# Accepted Manuscript

Self-assembly and metal-directed assembly of organic semiconductor aerogels and conductive carbon nanofiber aerogels with controllable nanoscale morphologies

Sally Turner, Brian Shevitski, Hu Long, Maydelle Lorenzo, James Marquez, Shaul Aloni, Virginia Altoe, Marcus A. Worsley, Alex Zettl



PII: S0008-6223(19)30726-2

DOI: <https://doi.org/10.1016/j.carbon.2019.07.039>

Reference: CARBON 14416

To appear in: *Carbon*

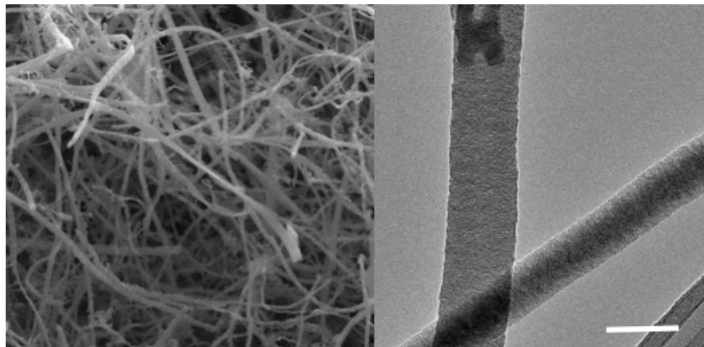
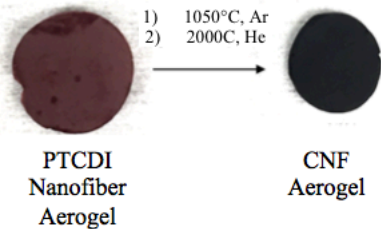
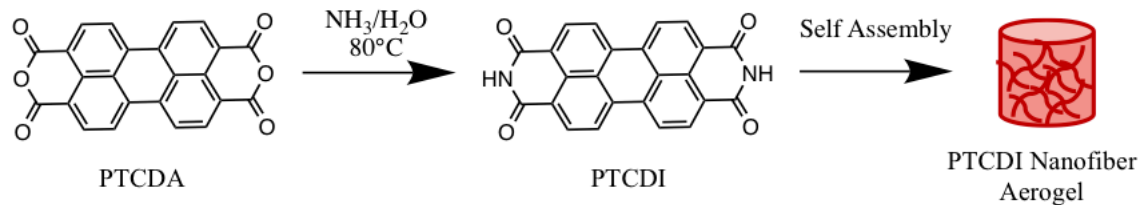
Received Date: 20 April 2019

Revised Date: 23 June 2019

Accepted Date: 11 July 2019

Please cite this article as: S. Turner, B. Shevitski, H. Long, M. Lorenzo, J. Marquez, S. Aloni, V. Altoe, M.A. Worsley, A. Zettl, Self-assembly and metal-directed assembly of organic semiconductor aerogels and conductive carbon nanofiber aerogels with controllable nanoscale morphologies, *Carbon* (2019), doi: <https://doi.org/10.1016/j.carbon.2019.07.039>.

This is a PDF file of an unedited manuscript that has been accepted for publication. As a service to our customers we are providing this early version of the manuscript. The manuscript will undergo copyediting, typesetting, and review of the resulting proof before it is published in its final form. Please note that during the production process errors may be discovered which could affect the content, and all legal disclaimers that apply to the journal pertain.



Highly Crystalline CNF Aerogel

# Self-Assembly and Metal-Directed Assembly of Organic Semiconductor Aerogels and Conductive Carbon Nanofiber Aerogels with Controllable Nanoscale Morphologies

Sally Turner<sup>a,b,c</sup>, Brian Shevitski<sup>b,c,d</sup>, Hu Long<sup>b,c</sup>, Maydelle Lorenzo<sup>a</sup>, James Marquez<sup>a</sup>, Shaul Aloni<sup>d</sup>, Virginia Altoe<sup>d</sup>, Marcus A. Worsley<sup>e</sup>, Alex Zettl<sup>b,c,f\*</sup>

<sup>a</sup> Department of Chemistry, University of California at Berkeley, Berkeley, California 94720, USA

<sup>b</sup> Department of Physics, University of California at Berkeley, Berkeley, California 94720, USA

<sup>c</sup> Kavli Energy NanoSciences Institute at the University of California, Berkeley and the Lawrence Berkeley National Laboratory, Berkeley, California 94720, USA

<sup>d</sup> Molecular Foundry, Lawrence Berkeley National Laboratory, Berkeley, California 94720, USA

<sup>e</sup> Physical and Life Science Directorate, Lawrence Livermore National Laboratory, Livermore, California, 94450, USA

<sup>f</sup> Materials Science Division, Lawrence Berkeley National Laboratory, Berkeley, California 94720, USA

## **Abstract**

A versatile and highly tunable synthesis for nanofiber aerogels based on the n-type organic semiconductor perylene tetracarboxylic diimide (PTCDI) is presented. PTCDI nanofiber aerogels are demonstrated to incorporate the organic semiconductor into a high surface area and porous morphology, and can also be graphitized to synthesize carbon nanofiber (CNF) aerogels by thermal annealing. Using this approach, CNF aerogels with variable density and crystallinity are synthesized. Furthermore, by incorporating metal salts into the synthesis, metal-directed assembly yields a variety of nanoscale morphologies. The selection of post-synthesis thermal treatment can result in metal-directed assembly of PTCDI aerogels, low crystallinity graphitic aerogels decorated with metal nanoparticles, or highly crystalline graphitic aerogels with controllable nanoscale morphologies. The high surface area and porosity afforded by the aerogel morphology coupled with the intrinsic properties of PTCDI or CNFs is important for improving their performance in a number of applications including energy storage and catalysis.

---

\* Corresponding author. Tel: (510) 642-4939. Email: [azettl@berkeley.edu](mailto:azettl@berkeley.edu) (Alex Zettl)

**Keywords:** Aerogel, carbon nanofiber, organic semiconductor, PTCDI, self-assembly, metal-directed assembly

## 1. Introduction

In recent years a wide variety of one dimensional (1D) nanofibers based on conductive carbonaceous materials, organic semiconductors, and inorganic materials have been explored due to their improved properties over their bulk counterparts<sup>1-10</sup>.

The organic semiconductor perylene tetracarboxydiimide (PTCDI) has attracted attention due to its high electron affinity and ability to self-assemble into nanostructures, and PTCDI nanofibers have been integrated into field-effect transistors, photovoltaics, and other electronic applications<sup>4,11-18</sup>. Carbon nanofibers (CNFs) are another type of 1D organic material with drastically different electronic properties than PTCDI nanofibers and possess excellent thermal and mechanical properties, as well as high electrical conductivity. These outstanding properties make carbon-based 1D nanofibers promising materials for energy storage applications such as supercapacitor electrodes, lithium ion battery anodes, catalytic supports, and composite energy materials<sup>19-23</sup>. Despite their high aspect ratios, PTCDI nanofibers and CNFs synthesized through classical vapor or solution methods possess surface areas below 20 m<sup>2</sup>/g and lack the high surface areas necessary for optimized performance in these applications<sup>3</sup>.

A larger surface area and porosity can be gained by incorporating CNFs and PTCDI nanofibers in aerogels. Aerogels are a class of three-dimensional materials characterized by their low density and textural properties including high surface area and porosity. The combination of the aerogel's textural properties and the intrinsic properties of the nanofiber has the potential to significantly improve the performance of these materials in a variety of applications by exposing active sites and facilitating mass transfer in the solid-state<sup>24-26</sup>.

Aerogels based on any organic semiconductor are scarcely reported in the literature, while CNF aerogels are becoming increasingly widely studied. For decades carbon aerogels have been studied utilizing the sol-gel polymerization of resorcinol and formaldehyde and subsequent pyrolysis gives rise to high surface area carbon monoliths with spherical nanoscale morphology and high electrical conductivity<sup>27-29</sup>. Due to the excitement surrounding the extraordinary properties of nanomaterials which can be imparted into aerogels, future frontiers in carbon aerogels utilize nanoscale morphologies including graphene, carbon nanotubes, and CNFs<sup>30-32</sup>.

CNF aerogels can be achieved through non-toxic and inexpensive means compared to their other nanoscale counterparts and have demonstrated potential in energy storage, electrocatalysis, and water treatment applications<sup>33-35</sup>. Current methods to synthesize CNF aerogels largely rely on templates for their synthesis and include hydrothermal carbonization of polysaccharides on tellurium nanowire templates, as well as biosynthesis by pyrolysis of a bacterial cellulose precursor<sup>36,37</sup>. Drawbacks to such methods include the cost of tellurium nanowires and need for additional template removal processing steps, as well as lack of control over the predetermined microstructure of the naturally occurring bacterial cellulose precursor. More recently, a method utilizing nanofibrillated cellulose derived from wood was developed, but a number of processing steps are required in order to synthesize CNF aerogels from wood pulp<sup>32</sup>. The aforementioned carbon aerogels, as well as graphene aerogels are assembled in one reaction step and subsequent heat treatment, and a more direct route to CNF aerogels is required to incorporate them into practical applications.

One relatively unexplored route to CNF aerogels utilizes the self-assembly of PTCDI molecules into nanofibers, where PTCDI nanofiber aerogels can serve of precursors for CNF aerogels<sup>38</sup>. Here, we report the first synthesis of PTCDI nanofiber aerogels from inexpensive and

commercially available perylene tetracarboxylic acid dianhydride (PTCDA). In this method, the synthesis of PTCDI, self-assembly of PTCDI into nanofibers, and gelation are combined into one single step to yield a PTCDI nanofiber aerogel. While the PTCDI nanofiber aerogel is useful on its own, it can also be graphitized in an inert atmosphere to yield CNF aerogels of tunable crystallinity. Furthermore, we demonstrate that incorporation of metal salts can drive metal-directed assembly of PTCDI and a number of nanoscale morphologies can be achieved. Through careful selection of post-synthesis thermal treatment, the metal salts can be reduced to metal nanoparticles in order to introduce additional active materials into the architecture, or aerogels can be annealed above the melting temperature of the metal to yield highly crystalline, purely graphitic, aerogels with controllable nanoscale morphologies.

## 2. Experimental

### 2.1 Synthesis PTCDI Nanofiber Aerogels

PTCDI nanofiber aerogels are synthesized by preparing a suspension of perylene-3,4,9,10-tetracarboxylic dianhydride (PTCDA) in water. The concentration of PTCDA is 100 mg/mL unless otherwise noted. A 1:6 by volume amount of  $\text{NH}_4\text{OH}:\text{H}_2\text{O}$  is added and the suspension is kept in a vial or cast into disk molds for gelation. Gelation takes place over 24hrs at 80 °C to yield PTCDI nanofiber hydrogels. Solvent is removed without surface tension by supercritical drying using  $\text{CO}_2$  or freeze-drying, yielding PTCDI nanofiber aerogels. Samples are prepared using supercritical drying unless otherwise noted.

### 2.2 Synthesis of CNF Aerogels

CNF aerogels are synthesized by high temperature treatment of PTCDI nanofiber aerogels in an inert atmosphere. PTCDI nanofiber aerogels are annealed at 1050 °C in Ar for 3

hrs to yield low crystallinity CNF aerogels. Subsequent firing at 2000 °C in He for 2 hours yields highly crystalline CNF aerogels.

### *2.3 Metal Directed Assembly of Aerogels*

Metal directed assembly of aerogels is achieved by dissolving 1.5mM of metal salt (NiCl<sub>2</sub>, HAuCl<sub>4</sub>, FeCl<sub>2</sub>, PdCl<sub>2</sub>, CoCl<sub>2</sub>) into the PTCDA suspension. A 1:6 by volume amount of NH<sub>4</sub>OH:H<sub>2</sub>O is added and the suspension is allowed to gel for 24hrs at 80 °C to yield metal directed assembled PTCDI hydrogels (M-PTCDI, M=Ni, Au, Fe, Pd, Co). Solvent is removed using supercritical CO<sub>2</sub> to yield M-PTCDI aerogels. M-PTCDI aerogels are annealed at 1050 °C in Ar followed by 2000 °C in He to yield M-CNF aerogels.

## **3. Results and Discussion**

### *3.1 PTCDI Nanofiber Aerogels*

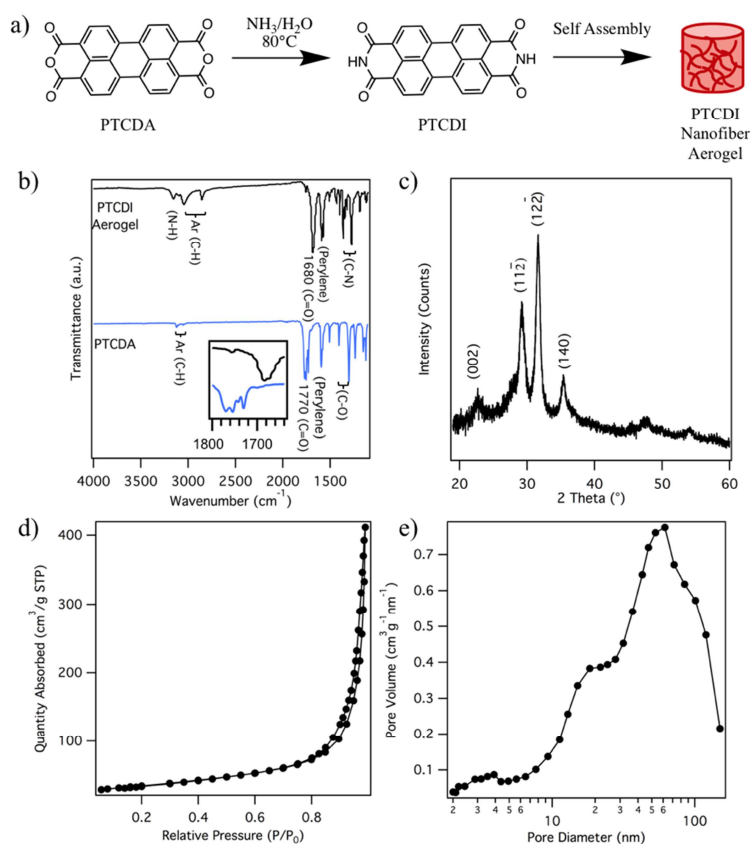


**Figure 1** a) Synthesis of PTCDI nanofiber aerogels b) FTIR spectra of PTCDA and as-produced PTCDI nanofiber aerogel c-e) XRD, nitrogen adsorption/desorption isotherm, and pore size distribution of PTCDI nanofiber aerogel, respectively.

As shown in **Figure 1a**, PTCDI nanofiber aerogels are synthesized by reacting PTCDA with ammonium hydroxide. PTCDI is known to self-assemble into nanofibers due to strong  $\pi$ - $\pi$  interactions between perylene cores<sup>12</sup>. At high concentrations of PTCDA, a large, entangled nanofiber network assembles and is capable of forming a freestanding hydrogel. In order to preserve the pore structure of the hydrogel during the drying process, solvent removal is performed using supercritical CO<sub>2</sub> or freeze-drying, yielding a PTCDI nanofiber aerogel. The successful conversion of PTCDA to PTCDI is verified using FTIR (**Figure 1b**). Peaks corresponding to the anhydride at 1775 and 1765 cm<sup>-1</sup> due to the asymmetric and symmetric C=O stretches disappear and are replaced with imide peaks from C=O, C-N, and N-H stretches at 1650, 1275, and 3130cm<sup>-1</sup>, respectively. Using XRD, the crystal structure of the nanofibers is

studied (**Figure 1c**). After the reaction, the product has prominent peaks at 22.6, 29.2, 31.6, and 35.4° corresponding to the (002), (11-2), (12-2), and (104) planes in PTCDI (monoclinic P21/n space group), respectively<sup>39</sup>.

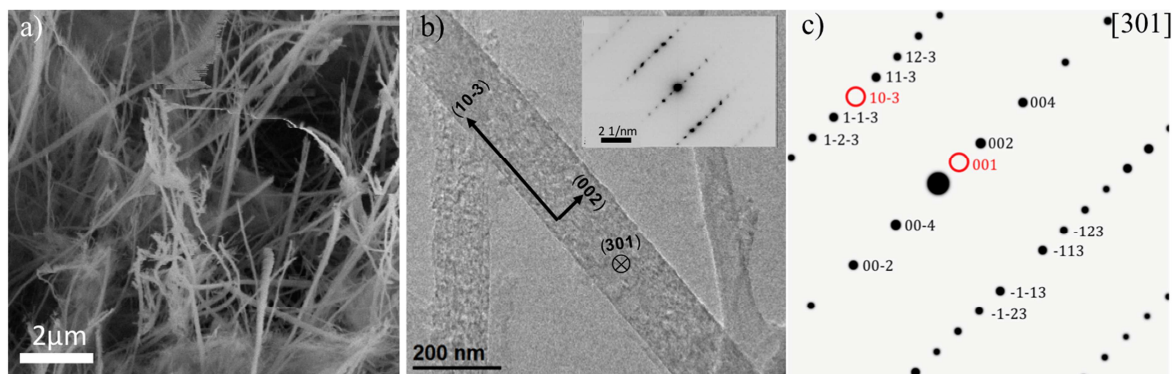


**Figure 2** a-b) SEM and TEM images of PTCDI nanofiber aerogels and diffraction pattern (inset), respectively. c) Simulated diffraction pattern of PTCDI nanofiber on the [301] zone axis. The missing reflections (red circles) in (c) appear as weak spots in the experimental diffraction pattern due to double diffraction. The diffraction pattern shows that the fibers have the monoclinic P21/c crystal structure and the fibers are aligned in the 10-3 direction.

The textural properties of the resulting aerogels are studied using nitrogen porosimetry. The nitrogen adsorption and desorption isotherms are shown in **Figure 1d** and form a Type IV (IUPAC definition) shape indicative of a mesoporous material. The calculated BET surface area is 123 m<sup>2</sup>/g, similar to other semiconducting aerogels in the literature<sup>40</sup>. The pore size distribution is studied using Barrett, Joyner, and Halenda (BJH) methods, indicating that the material is made up of predominantly mesopores (2-50nm) and macropores (greater than 50nm) with a very small contribution of micropores (less than 2nm) (**Figure 1e**). These textural properties are significantly impacted by the method used for solvent removal (**Figure S1, Table S1**), with supercritically dried samples having a higher surface area than PTCDI aerogels. The density of PTCDI nanofiber aerogels using a PTCDA concentration of 100 mg/mL is 89.4 mg/cm<sup>3</sup>, which is easily tuned by adjusting the PTCDA concentration resulting in densities between 323 and 22 mg/cm<sup>3</sup> (**Figure S2**). The minimum concentration of PTCDA required to reach a critical nanofiber entanglement to form a freestanding hydrogel cylinder is 25 mg/mL.

Formation of nanofibers is verified using SEM and TEM as shown in **Figure 2**. SEM reveals the three-dimensional (3D) nature of the aerogels which are composed of many micron long nanofibers (**Figure 2a**). PTCDI nanofiber aerogels contain a highly porous structure with a large amount of free-space, reflecting the low density of the material. Using TEM, individual nanofibers with widths between 100 and 200 nm are isolated and found to have a textured, as opposed to smooth, surface (**Figure 2b, S3**). SAED of isolated nanofibers is performed to determine PTCDI molecule orientation (**inset Figure 2b**). The experimental diffraction pattern matches that of a monoclinic  $p2c/1$  (space group 14) crystal in the  $[301]$  orientation, shown in the indexed simulated diffraction pattern in **Figure 2c**. The crystal orientation is annotated on the fiber, indicating PTCDI assembly along the nanofiber axis in the  $(10\text{-}3)$  direction and in the  $(002)$  direction along the nanofiber width. This is the first reported synthesis of a PTCDI nanofiber aerogel from the inexpensive and commercially available PTCDA compound. PTCDI is a well-known n-type organic semiconductor and semiconducting aerogels of any type have been scarcely reported in the literature, with those based on organic semiconductors even less reported. **Table S2** summarizes the properties of reported semiconducting aerogels. The PTCDI nanofiber aerogel can be used as a standalone material in applications such as photocatalysis, batteries, and electronic applications due to the intrinsic properties of the PTCDI building block<sup>16-18</sup>. In addition to these applications, PTCDI nanofiber aerogels can be used as precursors for the synthesis of CNF aerogels.

### *3.2 Carbon Nanofiber Aerogels*

Polycyclic aromatic hydrocarbons (PAHs) like PTCDI lack temperature stability and at high temperatures will undergo decomposition or pyrolysis. This property has led them to be used as sacrificial materials<sup>41</sup>. While PAHs fully oxidize in the presence of oxygen, in an inert environment both thermal decomposition and graphitization occur. This property is exploited in order to graphitize PTCDI nanofibers into CNFs. As outlined in **Figure 3a**, CNF aerogels are synthesized by thermal treatment of PTCDI nanofiber aerogels at 1050 °C followed by an

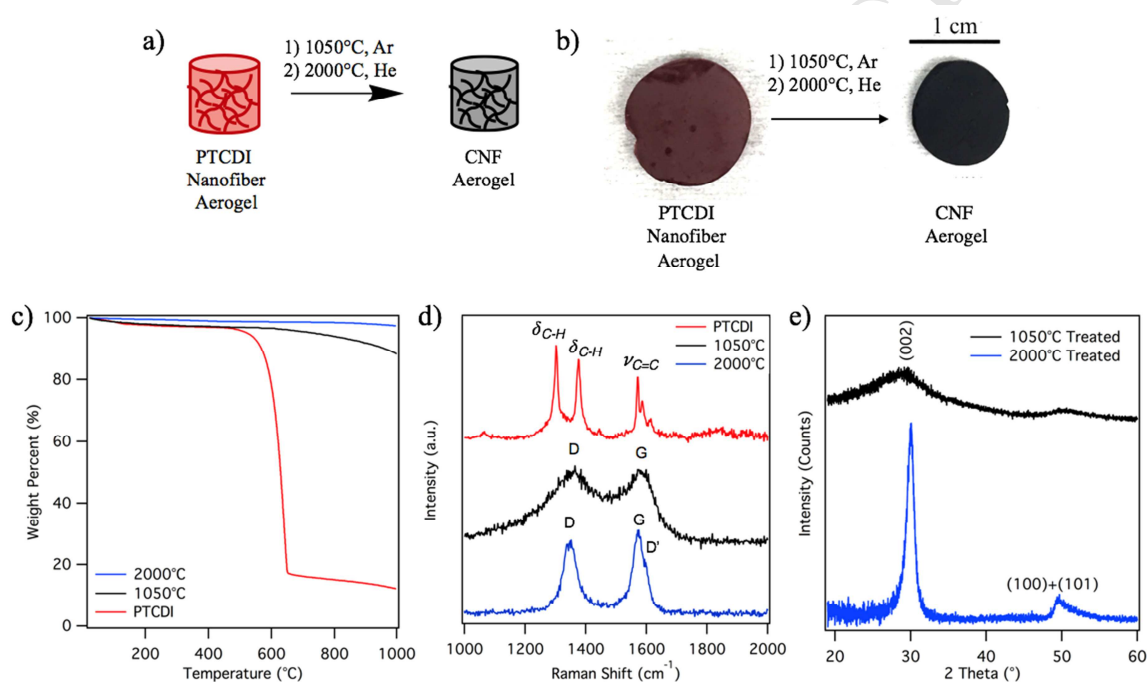


**Figure 3** a) Graphitization process from PTCDI nanofiber aerogel to CNF aerogel. b) Photographs of PTCDI nanofiber aerogel (left) and CNF aerogel (right). c-d) TGA in inert atmosphere and Raman spectra of PTCDI nanofiber aerogel, and CNF aerogels treated at 1050°C and 2000°C, respectively. e) XRD of CNF aerogels treated at 1050°C and 2000°C.

additional treatment at 2000 °C to increase crystallinity. TGA of PTCDI nanofiber aerogels conducted in an inert environment shows that a large mass change occurs between 400-600 °C, followed by a relatively stable mass until the maximum temperature of 1000 °C, indicating thermal decomposition and the formation of a more thermally stable phase (**Figure 3c**). Decomposition products are likely gaseous species such as carbon dioxide and carbon monoxide that are fully cleared from the aerogel. During the thermal 1050 °C treatment step there is a

visible color change from dark-red to black, further implicating the loss of perylene cores and formation of a graphitic phase (**Figure 3b**). Despite the clear chemical transformations, CNF aerogels treated at 1050 and 2000 °C still possess modest surface areas of 46 and 43 m<sup>2</sup>/g, respectively. This surface area is likely capable of increasing by post-synthesis activation using carbon dioxide or potassium hydroxide<sup>42,43</sup>. A comparison of the textural properties of CNF aerogels produced from this method to those from previously reported routes is shown in **Table S3**. Additionally, after treatment at 2000 °C, CNF aerogels are stable up to 750 °C in air and above 1000 °C in an inert atmosphere, making them suitable for high temperature applications (**Figure S4**).

Characterization of CNF aerogels treated at 1050 and 2000 °C is performed to study the chemical and structural transformations as a result of thermal annealing. Raman spectroscopy is a vital technique for characterization of graphitic materials and can be utilized to study crystallinity, defects, and conversion to graphitic phases<sup>44</sup>. Important Raman peaks in graphitic materials are the G peak due to the in-plane E<sub>2g</sub> phonon at 1575 cm<sup>-1</sup>, as well as the D peak at 1350 cm<sup>-1</sup> which requires a defect in order to activate and is indicative of the density of defects in a graphitic material. Before carbonization, the Raman spectrum of the PTCDI nanofiber aerogel has peaks at 1302, 1378 and 1572 cm<sup>-1</sup> due to C-H and C=C vibrations in the material (**Figure 3d**). After treatment at 1050 °C, the spectrum becomes that of a graphitic material with wide D and G peaks at 1362 and 1582 cm<sup>-1</sup>, indicating that graphitization occurs during the annealing step. However, the extremely broad D and G peaks indicate the low crystallinity of the material lack of a fully sp<sup>2</sup> hybridized structure. Subsequent treatment at 2000 °C results in extreme narrowing of the D and G peak consistent with enhancement in the crystallinity of CNF aerogels. Further chemical changes are probed using FTIR to verify loss of the vibrational

structure of PTCDI nanofibers during thermal treatment. In the FTIR spectrum, peaks previously referenced for PTCDI are lost after treatment at 1050 and 2000 °C and the classic IR spectrum for a graphitic structure is adopted which consists of a drifting baseline and lack of notable peaks (**Figure S4**).

After treatment at 1050 °C, XRD shows complete conversion of the PTCDI crystal structure in the PAH aerogel to a graphitic structure with a dominant peak at 30° corresponding to the graphitic (002) lattice plane and a minor peak around 50° which can be deconvoluted into peaks corresponding to the (100) and (101) planes<sup>45</sup> (**Figure 3e**). The broad (002) peak is indicative of the low crystallinity in the material leading to a distribution of interlayer spacings. Subsequent treatment at 2000 °C results in a narrow (002) peak with significantly increased intensity due to enhanced crystallinity in the material, in agreement with Raman spectroscopy. Using the Scherrer equation, the crystallite size for aerogels treated at 1050 and 2000 °C are calculated to be 1.0 and 8.7 nm, respectively<sup>46</sup>.

The chemical composition of CNF aerogels treated at 1050 and 2000 °C is studied using XPS (**Figure S5**). Treatment at 1050 °C results in a graphitic aerogel with 1.7% nitrogen remaining from the imide group. The C1s spectrum is made up of a dominant peak at 284.0 eV due to C=C bonding in the aerogels and minor peaks at 285.0, 286.4, and 288.4eV corresponding to C-O, C=O and O-C=O bonding, respectively<sup>47</sup>. Additionally, a shakeup feature at higher binding energy indicative of the sp<sup>2</sup> hybridized carbon is present and a small peak at lower binding energy of unknown origin is observed, but could potentially be due to a minor carbide species. CNF aerogels treated at 2000 °C contain a similar C1s spectrum and no nitrogen is detected in the sample after treatment, suggesting a purely carbon composition.

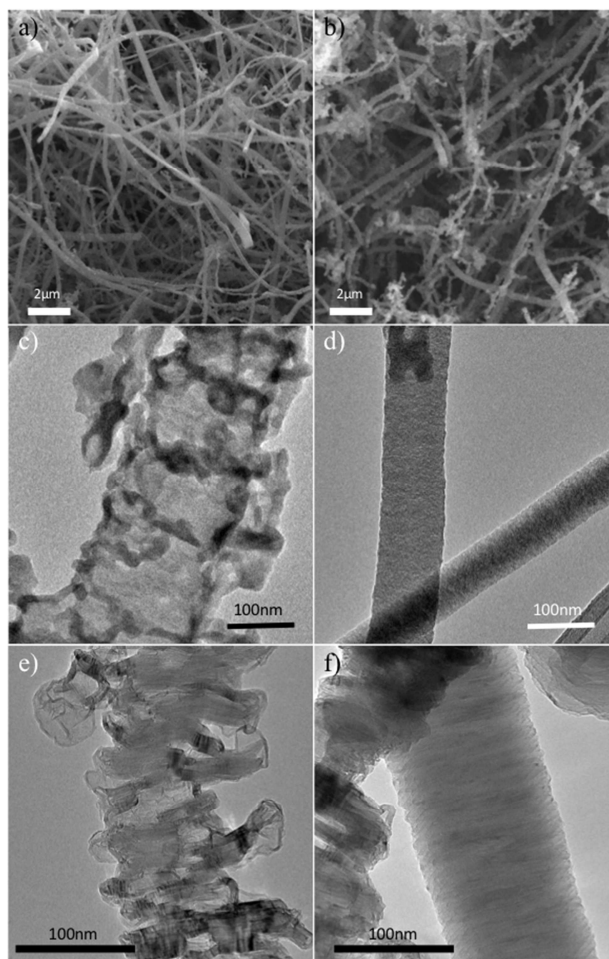


**Figure 4** a-b) SEM images of CNF aerogel treated at 1050°C and 2000°C, respectively c,d) TEM images of two difference CNF morphologies in aerogels treated at 1050°C e,f) TEM images of accordion-type and platelet-type CNFs present after 2000°C treatment, respectively.

CNF aerogels treated at 1050 and 2000 °C are structurally characterized using SEM and TEM (**Figure 4**). After 1050 °C firing, the high surface area, 3D morphology composed of nanofibers is largely maintained. CNFs have a range of widths predominantly between 100 and 200 nm and are several microns in length. After treatment at 2000 °C, the aerogel still maintains nanofiber morphologies, but nanofibers are packed more densely with less free space. This is also reflected in the density increasing from 45.4 mg/cm<sup>3</sup> after 1050 °C treatment to 82.8 mg/cm<sup>3</sup> after 2000 °C treatment.

TEM of nanofibers treated at 1050 °C shows that two distinct morphologies of nanofibers are present. As seen in **Figure 4c**, some nanofibers exhibit highly irregular structures that do not contain straight edges. This is likely due to the competing decomposition and graphitization processes taking place between 500-600 °C. The other type of nanofiber contains a much larger degree of ordering and quite smooth edges (**Figure 4d**). High magnification reveals that both types of nanofibers are made up of disordered graphitic layers with lattice fringes and a crystalline structure, in agreement with the broad (002) peak observed in XRD (**Figure S6**).

High temperature treatment at 2000 °C results in remarkable graphitization and increased crystallinity of nanofibers, with the two distinct nanofiber morphologies present at 1050 °C persisting in the aerogel despite graphitization (**Figure 4 e-f**). Both nanofiber morphologies exhibit stacking of the graphitic (002) plane perpendicular to the nanofiber axis as opposed to along the nanofiber axis as seen in the precursor PTCDI nanofiber aerogels. During thermal treatment, PTCDI is undergoing decomposition and graphitization simultaneously. Thus, it is hypothesized that these competing reactions, in addition to the high temperatures used for treatment, result in highly mobile atoms that reorganize into these structures, but the reason for deposition into these two distinct morphologies is unclear. Due the graphitic orientation perpendicular to the axis, nanofibers with smooth edges are a platelet-type carbon nanofiber and the irregular fibers have an accordion-type morphology. The aerogel is predominately composed of accordion-type morphology fibers, with fewer than one third of nanofibers being platelet type. Such platelet fibers have previously been reported but only synthesized using vapor phase methods as a result of catalytic processes during chemical vapor deposition<sup>48</sup>. To our knowledge, this is the first documentation of the accordion-type morphology of CNFs. Accordion-type CNFs maintain ordering perpendicular to the fiber axis, but also feature irregular stacking

approximately every 10-20nm along the nanofiber axis, leading to uneven nanofiber edges. Both platelet and accordion-type CNF morphologies have large domains composed of (002) planes, in agreement with the observation of an enhanced (002) diffraction peak in XRD.

In comparison with other CNF aerogel methods, the presented synthesis requires fewer steps than a chemosynthesis route requiring removal of tellurium templates and bioderived route requiring digestion steps of wood pulp. Additionally, the method is highly tunable due to the many parameters that can be controlled in the synthesis of the PTCDI precursor which can direct the density and textural properties and is unachievable in the predetermined architecture of bacterial cellulose derived CNF aerogels. Furthermore, the synthesis can be easily adapted to control the nanoscale morphology and to introduce additional active materials into the architecture, as described below. A comparison of parameters and properties of CNF aerogels synthesized from various methods is shown in **Table S3**.

### *3.3 Metal Directed Assembly of PTCDI and Graphitic Aerogels for Composite Materials and Controllable Nanoscale Morphologies*

In order to synthesize aerogels composed of controllable nanoscale morphologies, metal salts are incorporated into the PTCDA suspension during synthesis. The addition of a metal salt also serves to increase catalytic activity by forming composite materials. Using this approach, metal ions can interact with PTCDA and lead to metal directed self-assembly of PTCDI (M-PTCDI aerogels). The annealing temperatures can be carefully selected in order to synthesize graphitized aerogels decorated with metal nanoparticles, as well as aerogels with no trace of metal. We describe the synthesis and characterization of nickel directed assembly of CNF aerogels (Ni-CNF aerogels) by incorporation of  $\text{NiCl}_2$  into the PTCDA suspension. Additional

examples are contained in the Supporting Information and show that gold, cobalt, iron, and palladium can all be used for metal-directed assembly.

After gelation of the PTCDA suspension in the presence of  $\text{NiCl}_2$ , a dark-red hydrogel forms, which is then supercritically dried to form a Ni-PTCDI aerogel. As shown in the FTIR spectrum in **Figure S6a** one additional peak at  $3360\text{ cm}^{-1}$  emerges that is not present in PTCDI aerogels. This corresponds to Ni coordinated to the nitrogen in the imide. Additionally, shifting of peaks is observed as a result of Ni coordination resulting in the imide C=O shifting from  $1650\text{ cm}^{-1}$  to  $1690\text{ cm}^{-1}$ . After annealing at  $1050\text{ }^\circ\text{C}$  and  $2000\text{ }^\circ\text{C}$ , the expected graphene IR spectrum is obtained indicating loss of perylene cores and graphitization occurring during annealing. This is also supported by the recovery of the graphitic Raman spectrum after annealing (**Figure S7c**).

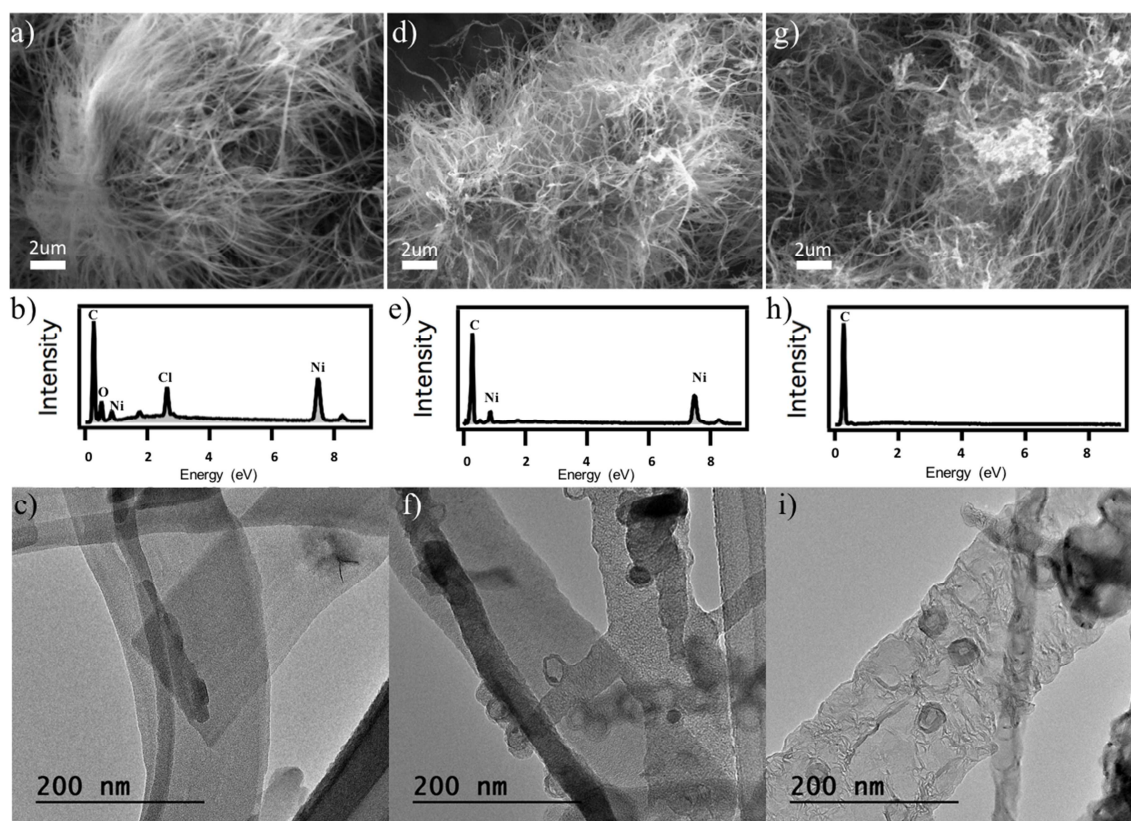


**Figure 5** SEM image, EDS spectrum and TEM image of a-c) Ni-PTCDI aerogel, d-e) Ni-CNF aerogel treated at 1050°C, g-i) Ni-CNF aerogel treated at 2000°C, respectively.

Using SEM, EDS and TEM, the 3D physical morphology and chemical composition of the M-PTCDI and thermally treated aerogels (M-CNF) are studied (**Figure 5**). SEM shows that Ni directed assembly results in an extremely dense nanofiber network in which nanofibers are closely packed in a bush-like morphology and many nanofibers originate from the same point. Additionally, EDS confirms the presence of nickel and chlorine in the M-PTCDI aerogels after supercritical drying (**Figure 5b**). Using TEM, M-PTCDI nanofibers are observed with widths around 100-200 nm and predominantly smooth edges (**Figure 5c**). After treatment at 1050 °C, SEM indicates that the nanofibers are more irregular and have more curvature after annealing. The composition is studied using EDS, which shows the presence of nickel and the elimination of chlorine in the aerogel (**Figure 5d,e**). At high temperatures and under inert or reducing conditions, metal salts such as  $\text{NiCl}_2$  will reduce and form metal nanoparticles, while chlorine is

released as HCl gas<sup>49</sup>. TEM imaging confirms the formation of Ni nanoparticles with diameters around 20nm, and assembly directly on CNFs (**Figure 5f**). A portion of Ni nanoparticles contain carbon shells and some areas contain hollow onions, in which a graphitic shell catalytically grows and redeposits prior to nickel evaporation. Nickel is commonly used as a chemical vapor deposition substrate in the growth of graphene due to its catalytic behavior<sup>50</sup>. Thus, it would be reasonable to expect nickel to play a catalytic role for the growth of additional carbon structures during thermal treatment, but hollow carbon onions are the only structures observed. However, CNF aerogels synthesized using H<sub>2</sub>AuCl<sub>4</sub> exhibit additional branching and assembly of Au nanoparticles directly the branch tips as a result of a catalytic role in their formation (**Figure S9h**).

Treatment at 2000 °C surpasses nickel's boiling point of 1450 °C, allowing a highly crystalline and fully graphitic CNF aerogel to be synthesized with altered nanoscale morphology. SEM shows that the 2000 °C Ni-CNF aerogel maintains the nanofiber morphology of its Ni-PTCDI and Ni-CNF 1050 °C aerogel counterparts at the microscale. EDS confirms that all nickel has evaporated and none remains after treatment at 2000 °C (**Figure 5g,h**). Additionally, TEM reveals the starkly different nanoscale morphology as the result of the Ni-directed assembly. As opposed to platelet and accordion type morphologies formed in the absence of NiCl<sub>2</sub>, Ni-CNF aerogels contain highly irregular stacking of the (002) lattice plane. At temperatures as high as 2000 °C, carbon atoms can readily diffuse, dissolve in nickel and be redeposited into irregular structures as seen in **Figures 5i, S8**. The large degree of disorder and nonuniform, packing of (002) domains leaves more vacant space in the CNF interior. This is significant because the irregularity results in an increased number of defects and can lead to additional active sites for catalysis<sup>51,52</sup>. This morphology also gives access to a larger accessible surface area for gas

storage in the nanofibers, while the high crystallinity maintains the good stability of CNFs. As a result of this phenomenon, the surface areas of Ni-CNF aerogels treated at 1050 °C and 2000 °C are 102 and 43 m<sup>2</sup>/g, respectively; increased relative to self-assembly without metal at 1050 °C treatment and comparable with classical self-assembly at 2000 °C treatment. Other nanoscale morphologies are formed using gold, cobalt, palladium and iron directed assembly including nanoflowers, nanoleaflets, and nanofibers of different widths (**Figure S9-S10**). These aerogels contain a broad range of compositions which can be controlled by selection of the post-synthetic thermal treatment and include 1) interfacing metals directly with the PTCDI organic semiconductor (M-PTCDI), 2) forming a composite aerogel with metal nanoparticles assembled on the low-crystallinity graphitic nanoassemblies (M-CNF-1050), and 3) forming aerogels entirely composed of the highly crystalline graphitic nanoassemblies of altered morphology (M-CNF-2000).

The compositions of M-PTCDI aerogels are summarized in **Table S4**. Hybrid structures of plasmonic metals and semiconductors possess intriguing optoelectronic properties and are capable of plasmon-enhanced performance in photocatalytic and solar energy applications<sup>53,54</sup>. Treatment at 1050°C leads to the formation of metal nanoparticles assembled on carbon nanofibers which have been demonstrated to have enhanced electrocatalytic activity, gas sensing performance, and lithium storage<sup>1,22,55,56</sup>. Lastly, metal content can be completely eliminated to yield a variety of nanoscale morphologies present in a highly crystalline aerogel and demonstrate the wide parameter range of the reported synthesis.

#### 4. Conclusion

In this study, we have demonstrated the synthesis of a new organic semiconductor aerogel based on PTCDI nanofibers, as well as a facile and highly tunable synthesis of CNF

aerogels by graphitization of PTCDI nanofiber aerogels. We show that careful selection of PTCDA concentration can control the final aerogel density and by choosing the annealing temperature for graphitization, the crystallinity of CNFs can be tuned. Furthermore, metal salts can be incorporated into the synthesis in order to synthesize aerogels with many different nanoscale morphologies. Selection of annealing temperature for metal directed assembly can lead to CNF-metal nanoparticle composites or highly graphitized, fully carbon aerogels with different nanoscale morphologies. Integrating organic semiconductor nanofibers and conductive CNFs into aerogels combines the intrinsic properties of the building blocks with the textural properties of the aerogel and represents a major step in improving and optimizing the performance of this class of materials for applications in photovoltaics, electrodes for energy storage applications, as well as gas storage applications, among others.

### **Acknowledgements**

This work was supported primarily by the Director, Office of Science, Office of Basic Energy Sciences, Materials Sciences, and Engineering Division, of the US Department of Energy, within the sp<sup>2</sup>-Bonded Materials Program (KC2207) (experimental design, synthesis, structural and chemical characterization). Work at LLNL was supported under the auspices of the US Department of Energy under contract No. DE-AC52-07NA27344 (supplementary synthesis and structural characterization). Work at the Molecular Foundry was supported by the Office of Science, Office of Basic Energy Sciences, of the US Department of Energy under Contract No. DE-AC02-05CH11231 (additional TEM and characterization). ST acknowledges the National Science Foundation Graduate Research Fellowship for support.

### **REFERENCES:**

- (1) Yang, D.-J.; Kamiyachik, I.; Youn, D. Y.; Rothschild, A.; Kim, I.-D. Ultrasensitive and Highly Selective Gas Sensors Based on Electrospun SnO<sub>2</sub> Nanofibers Modified by Pd

- Loading. *Adv. Funct. Mater.* **2010**, *20*, 4258–4264.
- (2) Tan, C.; Qi, X.; Liu, Z.; Zhao, F.; Li, H.; Huang, X.; Shi, L.; Zheng, B.; Zhang, X.; Xie, L.; et al. Self-Assembled Chiral Nanofibers from Ultrathin Low-Dimensional Nanomaterials. *J. Am. Chem. Soc.* **2015**, *137*, 1565–1571.
  - (3) Martin-Gullon, I.; Vera, J.; Conesa, J. A.; González, J. L.; Merino, C. Differences between Carbon Nanofibers Produced Using Fe and Ni Catalysts in a Floating Catalyst Reactor. *Carbon* **2006**, *44*, 1572-1580.
  - (4) Chou, Y.-H.; Lee, W.-Y.; Chen, W.-C. Self-Assembled Nanowires of Organic n-Type Semiconductor for Nonvolatile Transistor Memory Devices. *Adv. Funct. Mater.* **2012**, *22*, 4352–4359.
  - (5) Murthy, A. A.; Li, Y.; Palacios, E.; Li, Q.; Hao, S.; Distefano, J. G.; Wolverson, C.; Aydin, K.; Chen, X.; Dravid, V. P. Optically Active 1D MoS<sub>2</sub> Nanobelts. *ACS Appl. Mater. Interfaces* **2018**, *10*, 6799-6804.
  - (6) Chacko, D. K.; Madhavan, A. A.; Arun, T. A.; Thomas, S.; Anjusree, G. S.; Deepak, T. G.; Balakrishnan, A.; Subramanian, K. R. V.; Sivakumar, N.; Nair, S. V.; et al. Ultrafine TiO<sub>2</sub> Nanofibers for Photocatalysis. *RSC Adv.* **2013**, *3*, 24858.
  - (7) Sari, F. N. I.; Ting, J.-M. Direct Growth of MoS<sub>2</sub> Nanowalls on Carbon Nanofibers for Use in Supercapacitor. *Sci. Rep.* **2017**, *7*, 5999.
  - (8) Shin, J.; Choi, S.-J.; Lee, I.; Youn, D.-Y.; Park, C. O.; Lee, J.-H.; Tuller, H. L.; Kim, I.-D. Thin-Wall Assembled SnO<sub>2</sub> Fibers Functionalized by Catalytic Pt Nanoparticles and Their Superior Exhaled-Breath-Sensing Properties for the Diagnosis of Diabetes. *Adv. Funct. Mater.* **2013**, *23*, 2357–2367.
  - (9) Hoepfner, S.; Ratke, L.; Milow, B. Synthesis and Characterisation of Nanofibrillar Cellulose Aerogels. *Cellulose* **2008**, *15*, 121–129.
  - (10) Yan, P.; Brown, E.; Su, Q.; Li, J.; Wang, J.; Xu, C.; Zhou, C.; Lin, D. 3D Printing Hierarchical Silver Nanowire Aerogel with Highly Compressive Resilience and Tensile Elongation through Tunable Poisson's Ratio. *Small* **2017**, *13*, 1701756.
  - (11) Delgado, M. C. R.; Kim, E.-G.; Filho, D. A. da S.; Bredas, J.-L. Tuning the Charge-Transport Parameters of Perylene Diimide Single Crystals via End and/or Core Functionalization: A Density Functional Theory Investigation. *J. Am. Chem. Soc.* **2010**, *132*, 3375–3387.
  - (12) Balakrishnan, K.; Datar, A.; Oitker, R.; Chen, H.; Zuo, J.; Zang, L. Nanobelt Self-Assembly from an Organic n-Type Semiconductor: Propoxyethyl-PTCDI. *J. Am. Chem. Soc.* **2005**, *127*, 10496-10497.
  - (13) Kim, B. J.; Yu, H.; Oh, J. H.; Kang, M. S.; Cho, J. H. Electrical Transport through Single Nanowires of Dialkyl Perylene Diimide. *J. Phys. Chem. C* **2013**, *117*, 10743–10749.
  - (14) Zang, L. Interfacial Donor–Acceptor Engineering of Nanofiber Materials To Achieve Photoconductivity and Applications. *Acc. Chem. Res.* **2015**, *48*, 2705–2714.
  - (15) Wu, N.; Zhang, Y.; Wang, C.; Slattum, P. M.; Yang, X.; Zang, L. Thermoactivated Electrical Conductivity in Perylene Diimide Nanofiber Materials. *J. Phys. Chem. Lett.* **2017**, *8*, 292–298.
  - (16) Li, L.; Cai, Z. Structure Control and Photocatalytic Performance of Porous Conjugated Polymers Based on Perylene Diimide. *Polym. Chem.* **2016**, *7*, 4937–4943.
  - (17) Schon, T. B.; Tilley, A. J.; Kynaston, E. L.; Seferos, D. S. Three-Dimensional Arylene Diimide Frameworks for Highly Stable Lithium Ion Batteries. *ACS Appl. Mater. Interfaces* **2017**, *9*, 15631–15637.

- (18) Zhang, L.; Zhong, X.; Pavlica, E.; Li, S.; Klekachev, A.; Bratina, G.; Ebbesen, T. W.; Orgiu, E.; Samorì, P. A Nanomesh Scaffold for Supramolecular Nanowire Optoelectronic Devices. *Nat. Nanotechnol.* **2016**, *11*, 900–906.
- (19) Nan, D.; Huang, Z.-H.; Lv, R.; Yang, L.; Wang, J.-G.; Shen, W.; Lin, Y.; Yu, X.; Ye, L.; Sun, H.; et al. Nitrogen-Enriched Electrospun Porous Carbon Nanofiber Networks as High-Performance Free-Standing Electrode Materials. *J. Mater. Chem. A* **2014**, *2*, 19678–19684.
- (20) McDonough, J. R.; Choi, J. W.; Yang, Y.; La Mantia, F.; Zhang, Y.; Cui, Y. Carbon Nanofiber Supercapacitors with Large Areal Capacitances. *Appl. Phys. Lett.* **2009**, *95*, 243109.
- (21) Sebastián, D.; Suelves, I.; Moliner, R.; Lázaro, J.; Stassi, A.; Baglio, V.; Aricò, A. S. Optimizing the Synthesis of Carbon Nanofiber Based Electrocatalysts for Fuel Cells. *Applied Catal. B, Environ.* **2013**, *132*, 22–27.
- (22) Zhang, G.; Wu, H. Bin; Hoster, H. E.; Lou, X. W. (David). Strongly Coupled Carbon Nanofiber–Metal Oxide Coaxial Nanocables with Enhanced Lithium Storage Properties. *Energy Environ. Sci.* **2014**, *7*, 302–305.
- (23) Wilson, E.; Islam, M. F. Ultracompressible, High-Rate Supercapacitors from Graphene-Coated Carbon Nanotube Aerogels. *ACS Appl. Mater. Interfaces* **2015**, *7*, 5612–5618.
- (24) Gong, Y.; Fei, H.; Zou, X.; Zhou, W.; Yang, S.; Ye, G.; Liu, Z.; Peng, Z.; Lou, J.; Vajtai, R.; et al. Boron- and Nitrogen-Substituted Graphene Nanoribbons as Efficient Catalysts for Oxygen Reduction Reaction. *Chem. Mater.* **2015**, *27*, 1181–1186.
- (25) Fu, X.; Choi, J.-Y.; Zamani, P.; Jiang, G.; Ariful Hoque, M.; Mohamed Hassan, F.; Chen, Z. Co–N Decorated Hierarchically Porous Graphene Aerogel for Efficient Oxygen Reduction Reaction in Acid. *ACS Appl. Mater. Interfaces* **2016**, *8*, 6488–6495.
- (26) Sui, Z.; Meng, Q.; Zhang, X.; Ma, R.; Cao, B. Green Synthesis of Carbon Nanotube–Graphene Hybrid Aerogels and Their Use as Versatile Agents for Water Purification. *J. Mater. Chem.* **2012**, *22*, 8767.
- (27) Lu, X.; Nilsson, O.; Fricke, J.; Pekala, R. W. Thermal and Electrical Conductivity of Monolithic Carbon Aerogels. *J. Appl. Phys.* **1993**, *73*, 581–584.
- (28) Pekala, R. W. Organic Aerogels from the Polycondensation of Resorcinol with Formaldehyde. *J. Mater. Sci.* **1989**, *24*, 3221–3227.
- (29) ElKhatat, A. M.; Al-Muhtaseb, S. A. Advances in Tailoring Resorcinol-Formaldehyde Organic and Carbon Gels. *Adv. Mater.* **2011**, *23*, 2887–2903.
- (30) Worsley, M. A.; Pauzauskie, P. J.; Olson, T. Y.; Biener, J.; Satcher, J. H.; Baumann, T. F. Synthesis of Graphene Aerogel with High Electrical Conductivity. *J. Am. Chem. Soc.* **2010**, *132*, 14067–14069.
- (31) Yu, Z.; Qin, B.; Ma, Z.; Huang, J.; Li, S.; Zhao, H.; Li, H.; Zhu, Y.; Wu, H.; Yu, S. Superelastic Hard Carbon Nanofiber Aerogels. *Adv. Mater.* **2019**, *31*, 1900651.
- (32) Li, S.-C.; Hu, B.-C.; Ding, Y.-W.; Liang, H.-W.; Li, C.; Yu, Z.-Y.; Chen, W.-S.; Yu, S.-H. Wood-Derived Ultrathin Carbon Nanofiber Aerogels. *Angew. Chemie. Int. Ed.* **2018**, *57*, 7085–7090.
- (33) Liang, H.-W.; Wu, Z.-Y.; Chen, L.-F.; Li, C.; Yu, S.-H. Bacterial Cellulose Derived Nitrogen-Doped Carbon Nanofiber Aerogel: An Efficient Metal-Free Oxygen Reduction Electrocatalyst for Zinc-Air Battery. *Nano Energy* **2015**, *11*, 366–376.
- (34) Chen, L.-F.; Huang, Z.-H.; Liang, H.-W.; Guan, Q.-F.; Yu, S.-H. Bacterial-Cellulose-Derived Carbon Nanofiber@MnO<sub>2</sub> and Nitrogen-Doped Carbon Nanofiber Electrode

- Materials: An Asymmetric Supercapacitor with High Energy and Power Density. *Adv. Mater.* **2013**, *25*, 4746–4752.
- (35) Wang, L.; Schütz, C.; Salazar-Alvarez, G.; Titirici, M.-M. Carbon Aerogels from Bacterial Nanocellulose as Anodes for Lithium Ion Batteries. *RSC Adv.* **2014**, *4*, 17549.
- (36) Qian H.-S.; Yu, S.-H.; Luo L.-B.; Gong J.-Y.; Fei L.-F.; Liu, X.-M. Synthesis of Uniform Te@Carbon-Rich Composite Nanocables with Photoluminescence Properties and Carbonaceous Nanofibers by the Hydrothermal Carbonization of Glucose. *Chem. Mater.* **2006**, *18*, 2102-2108.
- (37) Wang, W.; Sun, Y.; Liu, B.; Wang, S.; Cao, M. Porous Carbon Nanofiber Webs Derived from Bacterial Cellulose as an Anode for High Performance Lithium Ion Batteries. *Carbon* **2015**, *91*, 56–65.
- (38) Liu, X.; Roberts, A.; Ahmed, A.; Wang, Z.; Li, X.; Zhang, H. Carbon Nanofibers by Pyrolysis of Self-Assembled Perylene Diimide Derivative Gels as Supercapacitor Electrode Materials. *J. Mater. Chem. A* **2015**, *3*, 15513–15522.
- (39) Deng, W.; Shen, Y.; Qian, J.; Cao, Y.; Yang, H. A Perylene Diimide Crystal with High Capacity and Stable Cyclability for Na-Ion Batteries. *ACS Appl. Mater. Interfaces* **2015**, *7*, 21095–21099.
- (40) Mohanan, J. L.; Arachchige, I. U.; Brock, S. L. Porous Semiconductor Chalcogenide Aerogels. *Science* **2005**, *307*, 397–400.
- (41) Turner, S.; Long, H.; Shevitski, B.; Pham, T.; Lorenzo, M.; Kennedy, E.; Aloni, S.; Worsley, M.; Zettl, A. Density Tunable Graphene Aerogels Using a Sacrificial Polycyclic Aromatic Hydrocarbon. *Phys. status solidi* **2017**, *254*, 1700203.
- (42) Yoon, S.-H.; Lim, S.; Song, Y.; Ota, Y.; Qiao, W.; Tanaka, A.; Mochida, I. KOH Activation of Carbon Nanofibers. *Carbon* **2004**, *42*, 1723-1729.
- (43) Chen, Y.; Liu, Q.; Wang, J. Carbon Dioxide Activated Carbon Nanofibers with Hierarchical Micro-/Mesoporosity towards Electrocatalytic Oxygen Reduction. *J. Mat. Chem. A* **2016**, *4*, 5553-5560.
- (44) Ferrari, A. C.; Meyer, J. C.; Scardaci, V.; Casiraghi, C.; Lazzeri, M.; Mauri, F.; Piscanec, S.; Jiang, D.; Novoselov, K. S.; Roth, S.; et al. Raman Spectrum of Graphene and Graphene Layers. *Phys. Rev. Lett.* **2006**, *97*, 187401.
- (45) Li, Z. Q.; Lu, C. J.; Xia, Z. P.; Zhou, Y.; Luo, Z. X-Ray Diffraction Patterns of Graphite and Turbostratic Carbon. **2007**, *45*, 1686-1695.
- (47) Holzwarth, U.; Gibson, N. The Scherrer Equation versus the “Debye-Scherrer Equation.” *Nat. Nanotechnol.* **2011**, *6*, 534–534.
- (48) Yoon, S.-H.; Lim, S.; Hong, S.; Mochida, I.; An, B.; Yokogawa, K. Carbon Nano-Rod as a Structural Unit of Carbon Nanofibers. *Carbon N. Y.* **2004**, *42*, 3087–3095.
- (49) Xia, B.; Lenggoro, I. W.; Okuyama, K. Preparation of Ni Particles by Ultrasonic Spray Pyrolysis of NiCl<sub>2</sub>·6H<sub>2</sub>O Precursor Containing Ammonia. *J. Mater. Sci.* **2001**, *36*, 1701–1705.
- (50) Obraztsov, A. N. Making Graphene on a Large Scale. *Nat. Nanotechnol.* **2009**, *4* (4), 212–213.
- (51) Ortiz-Medina, J.; Wang, Z.; Cruz-Silva, R.; Morelos-Gomez, A.; Wang, F.; Yao, X.; Terrones, M.; Endo, M. Defect Engineering and Surface Functionalization of Nanocarbons for Metal-Free Catalysis. *Adv. Mater.* **2019**, 1805717.
- (52) Jiang, Y.; Yang, L.; Sun, T.; Zhao, J.; Lyu, Z.; Zhuo, O.; Wang, X.; Wu, Q.; Ma, J.; Hu, Z. Significant Contribution of Intrinsic Carbon Defects to Oxygen Reduction Activity.

- ACS Catal.* **2015**, *5*, 6707-6712.
- (53) Gao, H.; Liu, C.; Jeong, H. E.; Yang, P. Plasmon-Enhanced Photocatalytic Activity of Iron Oxide on Gold Nanopillars. *ACS Nano* **2012**, *6*, 234–240.
- (54) Sheehan, S. W.; Noh, H.; Brudvig, G. W.; Cao, H.; Schmittenmaer, C. A. Plasmonic Enhancement of Dye-Sensitized Solar Cells Using Core–Shell–Shell Nanostructures. *J. Phys. Chem. C* **2013**, *117*, 927–934.
- (55) Huang, J.; Wang, D.; Hou, H.; You, T. Electrospun Palladium Nanoparticle-Loaded Carbon Nanofibers and Their Electrocatalytic Activities towards Hydrogen Peroxide and NADH. *Adv. Funct. Mater.* **2008**, *18*, 441–448.
- (56) Oh, H.-S.; Kim, H. Efficient Synthesis of Pt Nanoparticles Supported on Hydrophobic Graphitized Carbon Nanofibers for Electrocatalysts Using Noncovalent Functionalization. *Adv. Funct. Mater.* **2011**, *21*, 3954–3960.